Comparison of wavefront sensing and ablation imprinting for FEL focus diagnostics at FLASH2

In the following we compare along the caustic PMMA ablation imprints with beam intensity profiles back-propagated with various degrees of coherence from wavefront sensor (WFS) measured beam profiles. We carried out the measurements at wavelength of 7.92 nm, 13.48 nm and 13.5 nm with different FEL machine settings as shown in Table 1 of the article. For comparison we show intensity beam profiles simulated by the fully coherent WavePropaGator (WPG) software [1].

1. PMMA SAMPLE NO. 7

The measurements for PMMA sample no. 7 and the associated wavefront sensor measurements were carried out at a wavelength of 7.92 nm and using all 12 undulators. Young's double pinhole measurements were also made in the same shift. Nomarski microscope images of PMMA ablation imprints, back-propagated and WPG simulated intensity profiles along the caustic are compared in Fig. S1. The back-propagated intensities profiles using the maximum determined degree of coherence ($K = 0.57$ for $K_x = 0.71$, $K_y = 0.80$) and the minimum one ($K = 0.35$ for $K_x = 0.55$, $K_y = 0.64$) [2] are retrieved using MrBeam with the Gaussian coherence model. For comparison fully coherent back-propagated intensity beam profiles are shown as well. Unfortunately, only PMMA ablation imprints which were burned are available for comparison along the caustic. But nevertheless, there is a good match between the beam profiles shape and size. The structures in the boundary areas are weak and only seen at some z-positions along the caustic e. g. at 1 mm and 9 mm.

Table S1. *Fwhm* focus spot size at $\lambda = 7.92$ nm (PMMA sample no. 7) at the focus position.

degree of coherence		100 pulses averaged on CCD chip		mean value for 100 single pulses	
K_x	K_y	$fwhm_x$ (μm)	$fwhm_y$ (μm)	$fwhm_x$ (μm)	$fwhm_y$ (μm)
measured before PMMA ablation imprinting					
1.0	1.0	2.93 ± 0.01	4.42 ± 0.07	3.00 ± 0.11	4.25 ± 0.59
0.71	0.80	3.84 ± 0.01	5.56 ± 0.07	3.92 ± 0.15	5.20 ± 0.63
0.63	0.72	4.27 ± 0.01	6.06 ± 0.06	4.36 ± 0.17	5.70 ± 0.62
0.55	0.64	4.81 ± 0.01	6.59 ± 0.05	4.94 ± 0.19	6.28 ± 0.59
measured after PMMA ablation imprinting					
1.0	1.0	2.94 ± 0.01	3.66 ± 0.04	3.10 ± 0.21	3.83 ± 0.31
0.71	0.80	3.84 ± 0.01	4.41 ± 0.01	4.02 ± 0.23	4.64 ± 0.41
0.63	0.72	4.26 ± 0.01	4.87 ± 0.04	4.44 ± 0.22	5.12 ± 0.43
0.55	0.64	4.81 ± 0.01	5.45 ± 0.04	4.99 ± 0.22	5.70 ± 0.43

In Table S1 a more detailed analysis of the focus spot size using the Gaussian coherence function is put together. In the second column the resulting $fwhm$ focus spot sizes with fitting errors derived from a Gaussian fit of the back-propagated beam profiles for different degrees of coherence are shown for the measurement averaged on the CCD chip. In addition 100 individually measured pulses are back-propagated to the focus position, normalized and fitted in the same way. The resulting mean values of the $fwhm$ focus spot sizes with their standard deviations are collected in the third column. The upper part of Table S1 refers to WFS measurements taken immediately before the PMMA ablation imprints measurements, while the lower part is based on

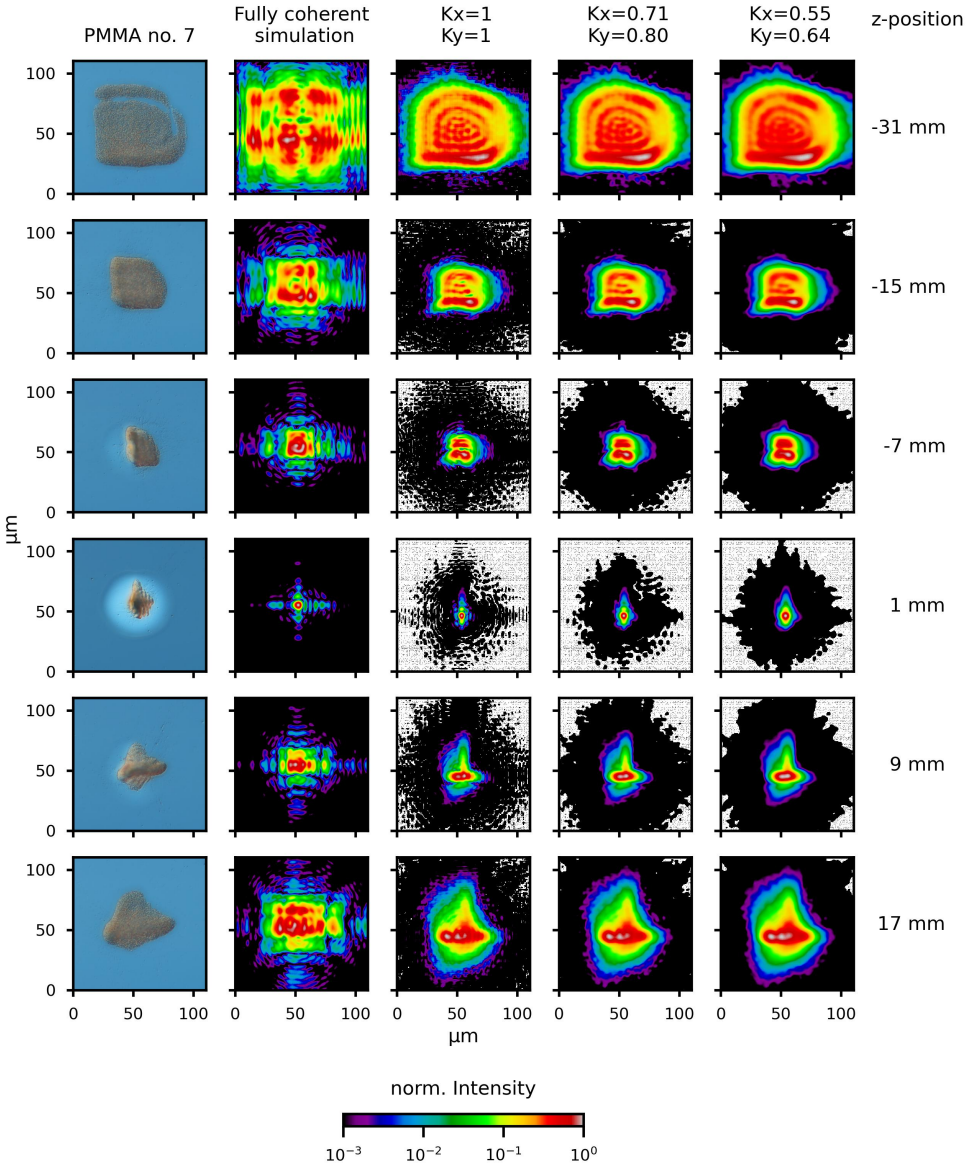

Fig. S1. Comparison of chosen PMMA imprints and beam intensity profiles simulated by WavePropaGator (WPG) or back-propagated with various degrees of coherence from WFS measured beam profiles. First column: Nomarski microscope images of PMMA imprints in sample no. 7 measured along the caustic. Second column: Simulated beam intensity profiles belonging to the corresponding z-positions, calculated using the fully coherent WPG software with a beam divergence of 80 μrad for measured mirror surface profiles. Last three columns: Back-propagated intensity profiles along the caustic retrieved from a measurement with 100 pulses averaged on the WFS CCD chip. Different degrees of coherence K_x in horizontal and K_y in vertical direction were used. Intensities are shown in logarithmic color scale to show the good agreement, also in boundary areas, of the beam profile shape and structure with the PMMA imprints. Propagation direction of the FEL light is from top to bottom. Focus position corresponds to $z = 0$ mm, wavelength is 7.92 nm with 12 undulators in use.

WFS measurements taken afterwards, approximately 3 hours later. In case of 100 pulses averaged on the CCD chip the focus spot sizes $fwhm_x$ and $fwhm_y$ remain almost unchanged over time ($\pm$0.3 %) or decrease by about 17 - 21 %, respectively. The same is observed for the mean value for 100 single pulses with a small spot size increase of 1 - 3.3 % for $fwhm_x$ and a slight decrease of 9 - 11 % for $fwhm_y$. The decrease of the focus spot size in horizontal direction can be explained by a small change of FEL pointing in y direction which leads to a slightly different beam path and therefore changed focusing of the KB optics in horizontal direction. The KB optics was not realigned during the shift to keep the measurements of all three methods comparable.

The decreasing degree of coherence in the back-propagations caused the size of the focal spot to increase similarly for both series of measurements, which were carried out before and after the PMMA ablation imprints measurements. The $fwhm_x$ focus size increase by about 31 % ($K = 0.57$; $K_x = 0.71$, $K_y = 0.80$), 45 % ($K = 0.45$; $K_x = 0.63$, $K_y = 0.72$), and 50 - 64 % ($K = 0.35$; $K_x = 0.55$, $K_y = 0.64$) compared to the fully coherent case. The increase of $fwhm_y$ is similar for the focus size in the y direction having 20 - 26 % ($K_x = 0.71$, $K_y = 0.80$), 33 - 37 % ($K_x = 0.63$, $K_y = 0.72$) and 49 % ($K_x = 0.55$, $K_y = 0.64$).

From the FAST simulations at 8.0 nm as shown in Fig. 2 of the article, a global degree of transverse coherence between 0.75 and 0.8 is expected for 12 undulators in use, assuming that the source is located in the last undulator section. The qualitative comparison of the WFS back-propagated intensity profiles as shown in Fig. S1 with the PMMA imprints allows us to assume that we had a similarly high degree of coherence, since otherwise the stripes visible at z-position 1 mm and 9 mm are washed out, as can be seen at lower degrees of coherence (last two columns). This is not quite in agreement with the results of the YDP measurements, which obtained a maximum global coherence of 0.56 (see third column of Fig. S1 and Table 1 of the article). It should be mentioned that some FEL electron and photon beam parameters were not measured or are unknown, therefore the FAST simulations required assumptions about e. g. the peak current of the electron beam, its pulse duration and shape as well as the emittance. In case of the FEL radiation the gain curve, the saturation length, the pulse duration and the angular divergence must be adopted in the simulations.

2. PMMA SAMPLE NO. 5

The measurements for PMMA sample no. 5 and the associated wavefront sensor measurements were carried out at a wavelength of 13.5 nm and the last 7 undulators in use. Young's double pinhole measurements were also performed in the same shift. In Fig. S2 Nomarski microscope images of PMMA ablation imprints from sample no. 5, back-propagated and WPG simulated beam profiles along the caustic are compared. The back-propagated intensity profiles are obtained from WFS measurements using the Gaussian coherence model with the maximum determined global degree of coherence ($K = 0.66$ for $K_x = 0.73$, $K_y = 0.91$), an intermediate one ($K = 0.56$ for $K_x = 0.67$, $K_y = 0.83$) [2], and for a fully coherent beam. Again, for this wavelength and undulator settings, there is good agreement along the caustic between the ablation imprints and the back-propagated intensity profiles with a high degree of coherence, as can be seen in the shape and size of the profiles as well as in the structures of the boundary regions. There is good agreement between the fully coherent WPG simulated and the fully coherent back-propagated intensity profiles.

Table S2. *Fwhm* focus spot size at $\lambda = 13.5$ nm (PMMA sample no. 5) at the focus position.

degree of coherence		100 pulses averaged on CCD chip		mean value for 100 single pulses	
K_x	K_y	$fwhm_x$ (μm)	$fwhm_y$ (μm)	$fwhm_x$ (μm)	$fwhm_y$ (μm)
measured before PMMA ablation imprinting					
1.0	1.0	3.78 ± 0.02	6.38 ± 0.1	3.77 ± 0.10	7.15 ± 0.72
0.73	0.91	4.75 ± 0.02	7.12 ± 0.1	4.74 ± 0.15	7.83 ± 0.67
0.67	0.83	5.10 ± 0.02	7.79 ± 0.09	5.09 ± 0.16	8.39 ± 0.60
0.61	0.72	5.52 ± 0.02	8.72 ± 0.08	5.51 ± 0.17	9.21 ± 0.50
0.55	0.69	6.04 ± 0.02	8.98 ± 0.08	6.03 ± 0.18	9.45 ± 0.48
measured after PMMA ablation imprinting (focus shifted by 6 mm upstream)					
1.0	1.0	3.83 ± 0.02	4.89 ± 0.03	3.91 ± 0.06	4.98 ± 0.11
0.73	0.91	4.80 ± 0.02	5.24 ± 0.03	4.91 ± 0.07	5.35 ± 0.14
0.67	0.83	5.16 ± 0.02	5.64 ± 0.03	5.27 ± 0.08	5.77 ± 0.18
0.61	0.72	5.60 ± 0.03	6.38 ± 0.04	5.72 ± 0.08	6.55 ± 0.24
0.55	0.69	6.14 ± 0.03	6.63 ± 0.04	6.27 ± 0.09	6.81 ± 0.25

A more detailed evaluation of the focus spot size using the Gaussian coherence function is collected in Table S2. In the second column the resulting $fwhm$ focus spot sizes with fitting errors derived from a Gaussian fit of the back-propagated beam profiles for different degrees of coherence are shown for the measurement averaged on the CCD chip. In addition 100 individually measured pulses are back-propagated to the focus position, normalized and fitted in the same way. The resulting mean values of the $fwhm$ focus spot sizes with the standard deviations are collected in the third column. The upper part of the table S2 is derived from measurements taken just before the PMMA ablation imprints, while the lower part is derived from measurements taken after the PMMA ablation imprints, approximately 4 hours later. For these measurements, the focus position was shifted by 6 mm upstream. In case of 100 pulses averaged on the CCD chip, $fwhm_x$ remains almost constant with an increase of only 1.1 - 1.6 %, while $fwhm_y$ is reduced by about 23 - 30 %. On the other hand, the changes in the case of mean value for 100 single pulses are somewhat larger, with an increase of 3.5 - 4.0 % for $fwhm_x$ and a decrease of 28 - 32 % for $fwhm_y$. This again shows the strong influence of FEL fluctuations, instabilities and changes of its pointing on the focus position as well as on the focus spot size. The large changes in the horizontal spot size indicate a greater horizontal instability of the FEL, resulting in a different FEL beam path and thus a different focusing of the KB optics system, which was not readjusted to keep the settings unchanged during a shift. The decreasing degree of coherence caused the

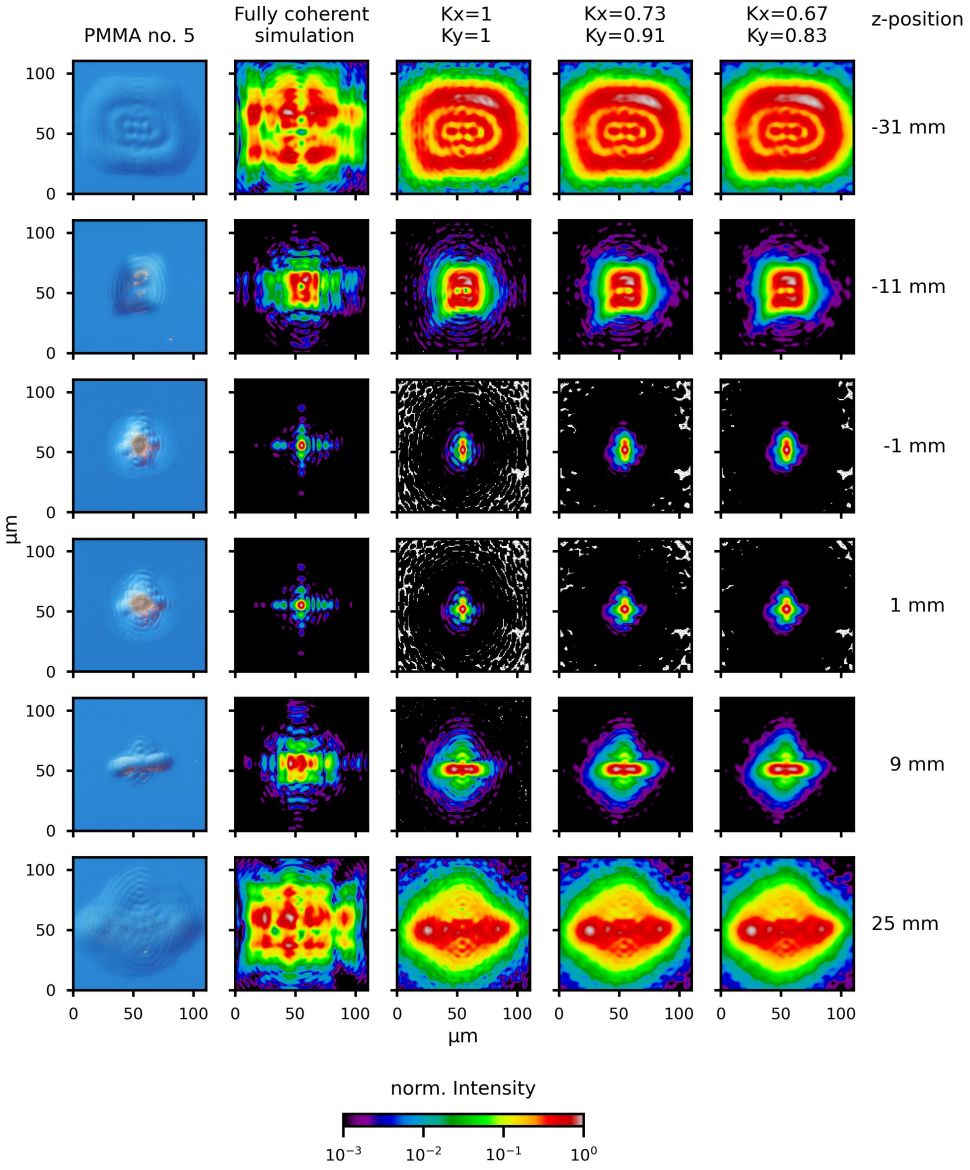

Fig. S2. Comparison of chosen PMMA imprints and beam intensity profiles simulated by WavePropaGator (WPG) or back-propagated with various degrees of coherence from WFS measured beam profiles. First column: Nomarski microscope images of PMMA imprints in sample no. 5 measured along the caustic. Second column: Simulated beam intensity profiles belonging to the corresponding z-positions, calculated using the fully coherent WPG software with a beam divergence of 80 μrad for measured mirror surface profiles. Last three columns: Back-propagated intensity profiles along the caustic retrieved from a measurement with 100 pulses averaged on the WFS CCD chip. Different degrees of coherence K_x in horizontal and K_y in vertical direction were used. Intensities are shown in logarithmic color scale to show the good agreement, also in boundary areas, of the beam profile shape and structure with the PMMA imprints. Propagation direction of the FEL light is from top to bottom. Focus position corresponds to $z = 0$ mm, wavelength is 13.5 nm with the last 7 undulators in use.

focal spot size to increase similarly for both measurements taken before and after the PMMA ablation imprints. The $fwhm_x$ spot size increases compared to the fully coherent spot size by about 26 % ($K = 0.66$; $K_x = 0.73$, $K_y = 0.91$), 35 % ($K = 0.56$; $K_x = 0.67$, $K_y = 0.83$), 46 % ($K = 0.44$; $K_x = 0.61$, $K_y = 0.72$), and 60 % ($K = 0.38$; $K_x = 0.55$, $K_y = 0.69$). In the case of $fwhm_y$ the increase in spot size is similar with 7 - 12 % ($K_x = 0.73$, $K_y = 0.91$), 15 - 22 % ($K_x = 0.67$, $K_y = 0.83$), 29 - 37 % ($K_x = 0.61$, $K_y = 0.72$), and 32 - 41 % ($K_x = 0.55$, $K_y = 0.69$).

From the FAST simulations at 13.5 nm as shown in Fig. 2 (red curve) of the article, a global degree of transverse coherence around 0.86 is expected for the last 7 undulators used, assuming that the source is located in the last used undulator section. A qualitative comparison between the ablation imprints (first column) and the back-propagated intensity profiles for K = 1 and K = 0.66 (third and fourth columns) suggests a high degree of partial coherence above 0.66, which is closer to the global coherence value of 0.86 obtained from the FAST simulation. Unfortunately, the agreement with the coherence values determined from Young's double pinhole measurements is not quite as good (see Table 1 of the article).

3. PMMA SAMPLE NO. 9

The measurements for PMMA sample no. 9 and the corresponding wavefront sensor measurements were performed at a wavelength of 13.48 nm with 12 undulators in use. The WFS measurements were performed immediately prior to the PMMA ablation imprints, and no WFS measurements were performed after the imprints. Young's double pinhole measurements were also carried out in the same shift. In Fig. S3 Nomarski microscope images of PMMA ablation imprints and back-propagated beam profiles along the caustic are compared. Here, a special FEL machine setup with 12 undulators was used, of which the last 6 undulators were tapered quadratic. The back-propagated intensity profiles are obtained from WFS measurements using the Gaussian coherence model with the maximum determined global degree of coherence ($K = 0.54$ for $K_x = 0.83$, $K_y = 0.65$), an intermediate one ($K = 0.45$ for $K_x = 0.72$, $K_y = 0.63$) [2], and for a fully coherent beam. Again, for this wavelength and undulator settings, there is a good match along the caustic between the ablation imprints and the back-propagated intensity profiles with a high degree of coherence, as can be seen in the shape and size of the profiles as well as in the structures of the boundary regions.

Table S3. *Fwhm* focus spot size at $\lambda = 13.48$ nm (PMMA sample no. 9) at the focus position.

degree of coherence		100 pulses averaged on CCD chip		mean value for 100 single pulses	
K_x	K_y	$fwhm_x$ (μm)	$fwhm_y$ (μm)	$fwhm_x$ (μm)	$fwhm_y$ (μm)
measured before PMMA ablation imprinting					
1.0	1.0	5.56 ± 0.03	6.15 ± 0.05	5.55 ± 0.62	6.12 ± 0.18
0.83	0.65	6.11 ± 0.03	8.08 ± 0.06	6.09 ± 0.58	8.04 ± 0.22
0.72	0.63	6.62 ± 0.03	8.28 ± 0.06	6.59 ± 0.55	8.24 ± 0.23
0.54	0.58	7.92 ± 0.02	8.87 ± 0.06	7.88 ± 0.48	8.83 ± 0.24

A more detailed evaluation of the focus spot size using the Gaussian coherence function is collected in Table S3. In the second column the resulting $fwhm$ focus spot sizes with fitting errors derived from a Gaussian fit of the back-propagated beam profiles for different degrees of coherence are shown for the measurement averaged on the CCD chip. In addition 100 individually measured pulses are back-propagated to the focus position, normalized and fitted in the same way. The resulting mean values of the $fwhm$ focus spot sizes with the standard deviation are collected in the third column. For both measurements the $fwhm_x$ spot size increase compared to the fully coherent spot size by about 10 % ($K = 0.59$; $K_x = 0.83$, $K_y = 0.65$), 19 % ($K = 0.45$; $K_x = 0.72$, $K_y = 0.63$), and 42 % ($K = 0.31$; $K_x = 0.54$, $K_y = 0.58$). In the case of $fwhm_y$ the increase in spot size is more uniform with 31 % ($K_x = 0.83$, $K_y = 0.65$), 35 % ($K_x = 0.72$, $K_y = 0.63$), and 44 % ($K_x = 0.54$, $K_y = 0.58$).

A qualitative comparison between the structures in the boundary areas of the ablation imprints (first column) and the back-propagated intensity profiles for K = 1 and K = 0.54 (second and third column), leads to expect a high degree of partial coherence above 0.54. From the FAST simulations at 13.5 nm as shown in Fig. 1 and Fig. 2 (red curve) of the article, a global degree of transverse coherence between 0.58 and 0.7 is expected for 12 undulators in use under the assumption that the source is located in the last undulator section. The agreement with the coherence values determined from Young's double pinhole measurements is quite reasonable (see Table 1 of the article) and much better than for PMMA sample no. 5. It should be mentioned that we used a special FEL machine setting for these measurements which are not included in the FAST simulations. Furthermore, some FEL electron and photon beam parameters were not measured or are unknown, therefore the FAST simulations required assumptions about e. g. the peak current of the electron beam, its pulse duration and shape as well as the emittance. In case of the FEL radiation the gain curve, the saturation length, the pulse duration and the angular divergence must be adopted in the simulations.

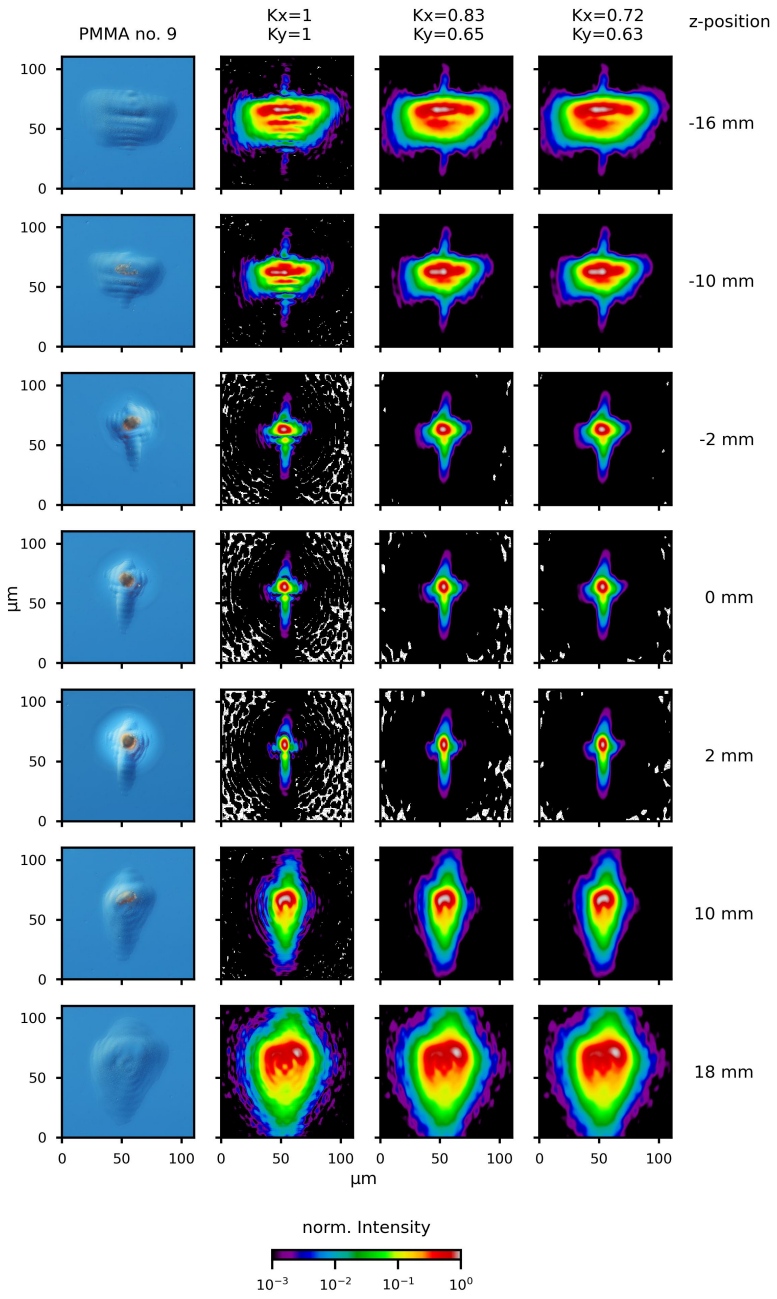

Fig. S3. Comparison of chosen PMMA imprints and intensity profiles back-propagated with various degrees of coherence from WFS measured beam profiles. First column: Nomarski microscope images of PMMA imprints in sample no. 9 measured along the caustic. Last three columns: Back-propagated intensity profiles along the caustic retrieved from a measurement with 100 pulses averaged on the WFS CCD chip. Different degrees of coherence K_x in horizontal and K_y in vertical direction were used with the Gaussian coherence function. Intensities are shown in logarithmic color scale to show the good agreement, also in boundary areas, of the beam profile shape and structure with the PMMA imprints. Propagation direction of the FEL light is from top to bottom. Focus position corresponds to $z = 0$ mm, wavelength is 13.48 nm with 12 undulators in use whereby the last 6 were quadratic tapered.

REFERENCES

1. L. Samoylova, A. Buzmakov, O. Chubar, and H. Sinn, "WavePropaGator: interactive framework for x-ray free-electron laser optics design and simulations," J. applied crystallography **49**, 1347–1355 (2016).
2. T. Wodzinski, M. Mehrjoo, M. Ruiz-Lopez, *et al.*, "Single-shot transverse coherence measurements with young's double pinholes at FLASH2," J. Phys. Commun. **4**, 075014 (2020).